**Title**
Semi-automatic Segmentation of the Prostate by MR Fat Fraction Map

**Permalink**
https://escholarship.org/uc/item/7bs8b8k1

**Author**
Korn, Natalie Johanna

**Publication Date**
2014

Peer reviewed|Thesis/dissertation

Semi-automatic Segmentation of the Prostate
by MR Fat Fraction Map

by

Natalie Korn

THESIS

Submitted in partial satisfaction of the requirements for the degree of

MASTER OF SCIENCE

in

Biomedical Imaging

in the

GRADUATE DIVISION

of the

UNIVERSITY OF CALIFORNIA, SAN FRANCISCO

Acknowledgments

# Semi-automatic Segmentation of the Prostate by MR Fat Fraction Map

*Natalie Korn*

The purpose of this study was to create a semi-automatic segmentation of the prostate for an accurate estimation of prostate volume and modeling of longitudinal changes in patient data. Segmentation algorithms are available based on axial T2-weighted imaging, but decrease in accuracy in abnormal or treated data, and can be expensive. In this work, we segment based on a fat fraction map (FF map), due to the smaller change in image intensities after treatment and large contrast between the prostate and surrounding fatty tissue. The algorithm consists of five parts: a global filtering of the image; region growth from a predetermined seed point; spline interpolation of the region-enclosing polygon; a comparison of distances between boundary points on adjacent slices; and backward mapping to an upsampled plane with a final volume extrusion. Image artifact is removed by morphological opening after the initial region growth, and by removing boundary points with a shortest distance to an adjacent slice boundary greater than a predetermined threshold. FF maps emphasizing low resolution in favor of high contrast (FF_hc maps), and FF maps emphasizing low contrast in favor of high resolution (FF_hr maps) using different acquisition parameters were tested for accuracy against a manual segmentation drawn on a T2-weighted image in fourteen patients receiving a multiparametric MR exam for confirmed or suspected prostate cancer. There was no significant difference in the volumes recorded from the trial data for the semi-automatic segmentation of the FF_hr map and manual segmentation of the axial T2-weighted image ($n=14$, $p<0.84$, paired students t-test), but FF_hr map segmentation had a trend to underestimate the size of the prostate gland. The FF_hc

map segmentation volumes were significantly different from those of the axial T2-weighted images (n=14, p<0.03, paired student's t-test). The segmentations of FF_hc maps showed psoas muscle invasion into the prostate region as the most common artifact due to the anatomic proximity and signal similarity, and both FF map types showed ambiguity as the prostate base abuts the bladder, leading to both over- and underestimation. This quick segmentation using FF_hr maps creates accurate prostate volume estimations and should be pursued.

Proposal Contents:                                              Page

Chapter 1: Introduction

Prostate cancer is the second-most prevalent cancer diagnosed in American men. However, it is associated with very low mortality in comparison to other forms of cancer[1], and can reside in the body for years without progression. The ability to distinguish between prostate cancers that will progress rapidly and those that will remain stagnant is an active area of research, and a combinatory assessment of blood work, pathology, and imaging is being explored to determine patient-specific cancerous potential.

One of the most common methods of estimating prostate growth in diagnosed populations is through testing of serum prostate-specific antigen (PSA) levels. However, the usefulness of PSA tracking is controversial because of the ambiguous correlation of PSA levels with both cancerous and benign prostate growth[2]. A more robust metric gaining popularity in the clinic is PSA density (total PSA/ prostate volume). A high PSA in a large prostate (low density) is less likely to contain cancer than a similar PSA in a small prostate (high density) [2]. However, an estimation of prostate volume is necessary to calculate PSA density.

At biopsy diagnosis of prostate cancer, advanced imaging techniques have been shown to better the ability to improve the assessment of cancer extent, as well as provide a measure of aggressiveness (Gleason grade). In particular, the multiparametric MRI (mpMRI) has been explored as a method of determining high-resolution anatomical changes, as well as cell density, metabolism, and perfusion throughout the prostate[3]. The addition of a semi-automatic segmentation of the prostate to create a volume estimate and monitor size changes may add to the information patients receive during

an MRI. Because MRI carries no radiation dosage, this exam is particularly useful for patients with low- and intermediate-grade cancer pursuing a treatment regimen known as active surveillance[3]. Active surveillance arose in popularity with the knowledge that because some prostate cancers do not progress and treatment commonly incurs negative side effects[4], launching into therapy may be more detrimental to patients with low-risk disease than closely monitoring the trajectory of the cancer[1]. In a combination of serum and imaging data, patients pursuing active surveillance typically receive serial PSA testing, which could be matched to an MRI exam for accurate PSA density.

A precise segmentation could also be combined with biopsy to improve pathological data collection. Currently, MR- and ultrasound-guided biopsies are used to more accurately sample the gland, but positioning is largely visual and prone to operator error[5]. A segmentation that could determine the placement and boundaries of the prostate gland could be created during an MR-guided biopsy and used to align the biopsy to a suspicious region.

Currently, estimates of prostatic volume in the clinic vary around a common theme of estimating an ellipsoid based on three manual measurements by a radiologist: a long-axis measurement in the oblique S/I direction, a short-axis measurement in the A/P direction, and a transverse measurement in the R/L direction[6]. An ellipsoidal volume is estimated from these measurements, but does not change in shape with abnormalities in the gland.

Creating a volume of the prostate based on the unique shape of each slice in an MR image accounts for slice-by-slice changes in the shape of the prostate. Furthermore, it will be particularly helpful in longitudinal studies. Using the standard

clinical practice, an increase in prostate volume cannot be localized to a specific part of the prostate. However, building a volume by individual slices can show changes in volume in localized regions between a patient's past and current exam, and correlate with functional imaging data. Areas of gland expansion in between clinical visits could be targeted in MR-guided biopsies.

In this work, we present a method of semi-automatic prostate segmentation based on an MR fat fraction (FF) map. The FF map creates signal intensity based on amount of fat, leaving the low-fat prostate dark and surrounding visceral fat bright. This novel method uses region growth paired with spline interpolation to delineate the prostate from the surrounding fatty tissue. Each slice creates highly accurate area estimations, and the 3D volume can show overall gland shape, as well as changes in the gland in longitudinal studies.

Chapter 2: Materials and Methods

*2.1 Subjects*

This prospective study was approved by our institutional review board and was compliant with the Health Insurance Portability and Accountability Act. Written, informed consent was obtained from all participants. Fourteen patients receiving MR examinations of the prostate were studied between May and August of 2014. Patients presented with suspected prostate cancer, as indicated by either elevated levels of serum prostate-specific antigen (PSA) (median=6.49, range 1.50 to 10.31), biopsy-proven prostate cancer, or both. The patients' mean age was 66.6 years, ranging from 55 to 78 years old. One patient had undergone hormone therapy; all other patients had received no treatment. Nine patients had a biopsy result of Gleason Score 3+3, two patients had a result of 3+4, one patient had a result of 4+3, and two patients had negative biopsies.

*2.2 MR Acquisition Methods*

All images were acquired using a 3T MR scanner (GE Healthcare, Waukesha, WI, USA) equipped with an eight-channel phased-array for the pelvis and an endorectal coil encased in a balloon probe (Bayer Healthcare, Warrendale, Pa, USA). A perfluorocarbon compound (3M, St. Paul, MN, USA) was used to inflate the balloon probe to reduce artifacts due to susceptibility[7].

The mpMRI examination of the prostate included high-resolution anatomic imaging provided by a three-dimensional fast spin-echo (FSE) pulse sequence with parallel imaging and extended echo train acquisition (CUBE)[8], reconstructed in the sagittal, coronal, and oblique axial views. Along with the CUBE imaging, an oblique

axial T2-weighted image (512x512, TR/TE=6350/103 ms) was acquired through the prostate to use for prescribing and visualizing anatomy correlated with the functional imaging sequences.

The mpMRI also includes three types of functional imaging, measured in the oblique axial direction: diffusion-weighted imaging (DWI), dynamic contrast-enhanced (DCE) imaging, and spectroscopy. DWI measures water motion, depending on gradient strength and duration known as a 'b-value'. It is useful in differentiating high-grade tumors from healthy tissue, as high cell density, a characteristic of high-grade tumors, restricts water motion[9]. DCE measures uptake and washout of an injected contrast agent over time, and is valuable in detecting both low-grade and high-grade cancers, as both initial breakdown of the prostate's glandular basement membrane (typical of low-grade disease) and angiogenesis (typical of high-grade disease) increase the rate of uptake and washout[10]. Spectroscopy provides complimentary information on the metabolic activity throughout the prostate, with Gleason score increasing with increases in the ratio of choline and creatine concentrations over citrate concentration[11].

An oblique axial 3D Iterative Decomposition and Echo Asymmetry with Least-squares estimation (IDEAL) sequence[12] was used to create high contrast between the prostate and surrounding tissue, to segment the prostate and to align with functional imaging metrics. The IDEAL sequences' prescriptions are copied from the oblique axial T2-weighted image to correlate with the anatomy. The IDEAL sequence was selected for segmentation of the prostate due to its utility in creating a fat fraction map that accounts for both B0 and B1 inhomogeneities by acquiring three images with relative phases of fat and water[12]. This three-point Dixon method is optimized in IDEAL imaging

for maximal signal in the resultant fat-only and water-only images. The FF map exploits the anatomic fat margins surrounding the prostate, which create a bright boundary. The prostate gland has a very low fat content, and appears dark in contrast, as in Figure 1.
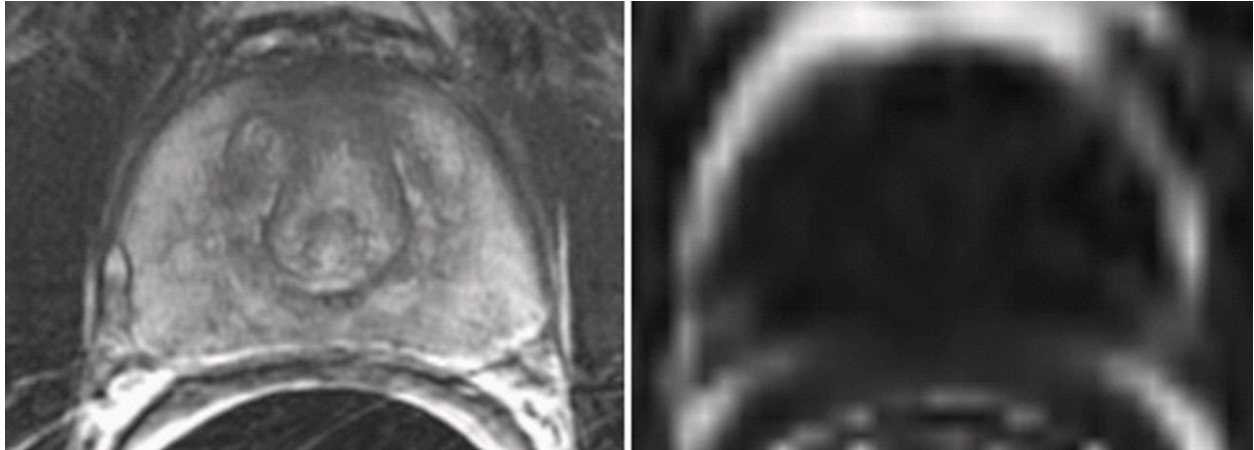


Figure 1: An a) oblique axial T2-weighted image of the prostate on an untreated patient from the sample population, and b) an oblique axial FF map created in the same location on the same patient. A B

The IDEAL sequence implemented needed to be sufficiently short such that it could be incorporated into a clinical mpMRI exam without significantly lengthening the exam duration. The initial IDEAL sequence parameters (TR/TE=6900/min full ms; 256x128; echo train length=3; 32 locations/slab; phase acceleration=2, NEX=.75) used a field of view (FOV) of 50 cm, phase FOV of .6, and slice thickness of 3 mm. Scanning required 28 seconds, and prescans required from 15 to 60 seconds, for a total added time of 88 seconds, which was clinically feasible. This sequence created images with high image contrast but had a low spatial resolution (high-contrast: IDEAL_hc).

However, due to a need to have an improved delineation of the prostate boundaries in-plane, the IDEAL sequence was tested with higher resolution (high resolution: IDEAL_hr). The IDEAL_hr sequence parameters (TR/TE = 7800/min full ms; 256x128; echo train length=3; 32 locations/slab; phase acceleration=2, NEX=1) used an

FOV of 36 cm, phase FOV of .8, and slice thickness of 3 mm. The scan time was 54 seconds, and prescans required from 15 to 60 seconds, for a total added time of 114 seconds. To determine the improvement in segmentation provided by higher spatial resolution IDEAL imaging, both the original, high contrast sequence (IDEAL_hc) and the higher resolution sequence (IDEAL_hr) were acquired on all 14 patients.

The IDEAL sequence produces FF maps by isolating signals of fat and water from the various echo times, and combining into a percentage—or fraction—of fat. Because fat and water are the most prevalent signals acquired, the fat fraction is defined as the signal from fat divided by the product of the signals from fat and water. Production of a FF map is accomplished using GE service software. The FF map was generated for each patient from the IDEAL_hc sequence emphasizing high contrast (FF_hc), and the high-resolution sequence IDEAL_hr (FF_hr).

To compare the volumes created from the semi-automatic segmentation algorithm, a gold standard of manual segmentation was performed on an axial T2-weighted image for each patient. The T2-weighted image was chosen for maximal anatomic detail easily visible to the human eye. In the manual segmentation, a region of interest (ROI) was drawn on every slice of the prostate as determined by the user. The volume was recorded and added to the slice stack to form the full volume of the prostate. A single user performed all manual segmentations to correct for interoperator variability.

*4.3 Algorithm Design*

The segmentation algorithm developed in this work was composed of five steps, including methods of boundary delineation and methods for artifact reduction. The

image setup contains all user input and global filtering. Following setup, a region growth method was used to formulate a general outline of the prostate region. From the shape defined by the region growth, a piecewise cubic spline interpolation smoothens the enclosing polygon. The spline of each image slice was tested for its lateral distance from the boundary of an adjacent slice. Lastly, a volume calculation was made after upsampling in three dimensions and converting pixel area to physical space. The algorithm was written in MatLab (MatLab R2012a, The MathWorks Natick, MA 2012) and executable at the command line. The full algorithm outline is shown in Figure 2.

To begin image setup, the algorithm requires input of an image stack, which is zoomed to the center 50x50 pixels for the viewing ease of the user. The user is prompted to input the two slice numbers representing the furthest extents of the prostate: noted 'start' and 'end'. The remainder of the algorithm will only be executed on image slices included and between start and end positions provided. Following the user input, a 3x3 median filter is employed to smooth and connect the fatty boundary surrounding the prostate. The median filter was chosen for its ability to remove signal outliers without averaging noise into the resulting intensity, as shown in Figure 3. It is therefore useful when noisy pixels deviate largely compared to true signal values. The size of the median filter was determined by the typical width in pixels of the fatty tissue between the prostate and surrounding musculature.

The smoothed image is fed to a region growth technique[13], which begins at a predefined seed point 20 pixels anterior to image center. The seed point is optimized from observation of image prescription, wherein the technologist places the image center in the rectum. Because all exams include use of the endorectal probe inflated
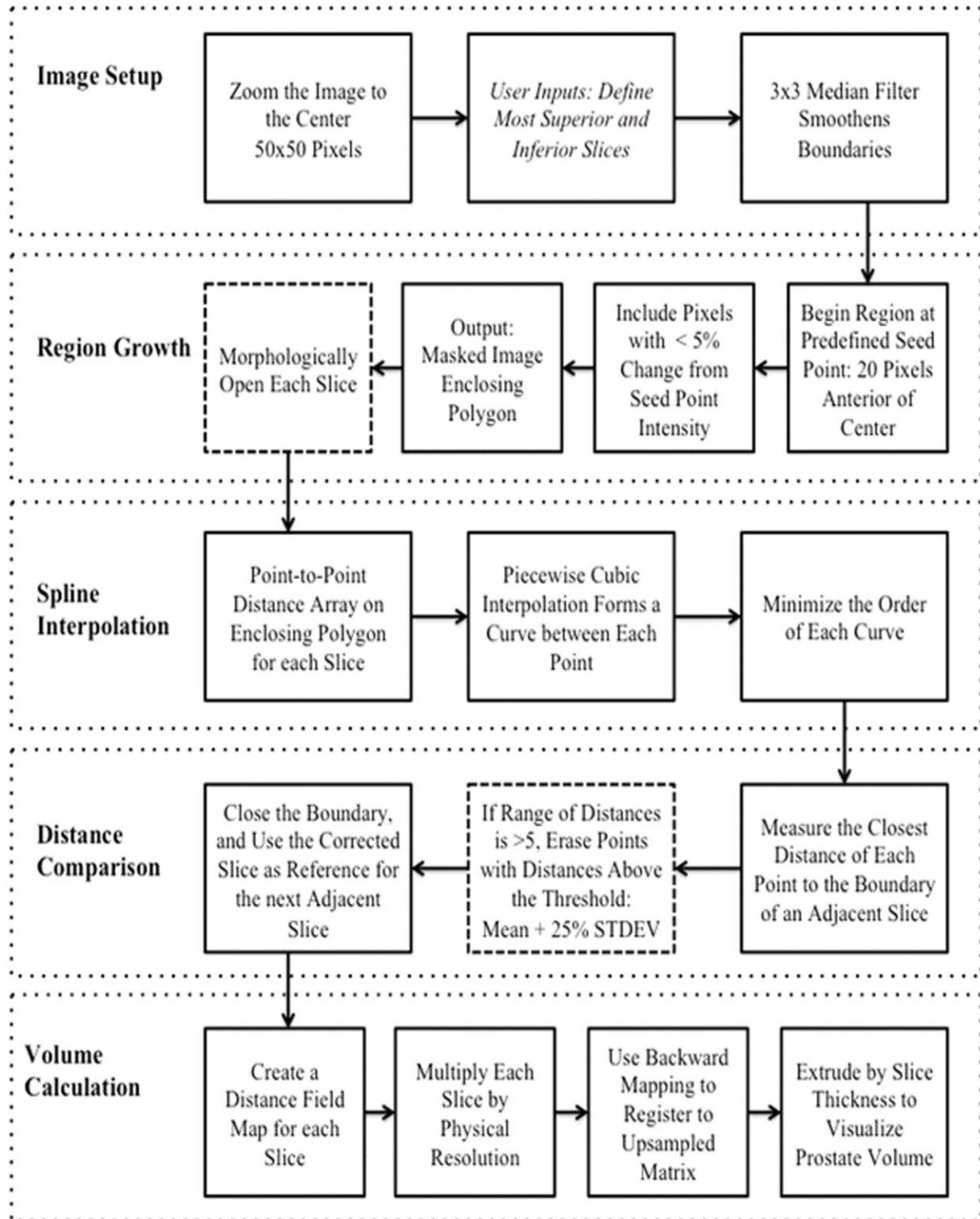
Figure 2: Semiautomatic segmentation algorithm in full. Italicized steps require user input, and dashed boxes indicate steps that eliminate artifact.

with a perfluorocarbon compound[7], the rectal size and location in the image is reproducible. Because the prostate sits immediately above the inflated rectum in this oblique axial prescription, the prostate is typically located at 10 pixels anterior to the center. 20 pixels anterior to image center was chosen so that the seed lands in the apex of the prostate, which can be small and located farther from the rectum.
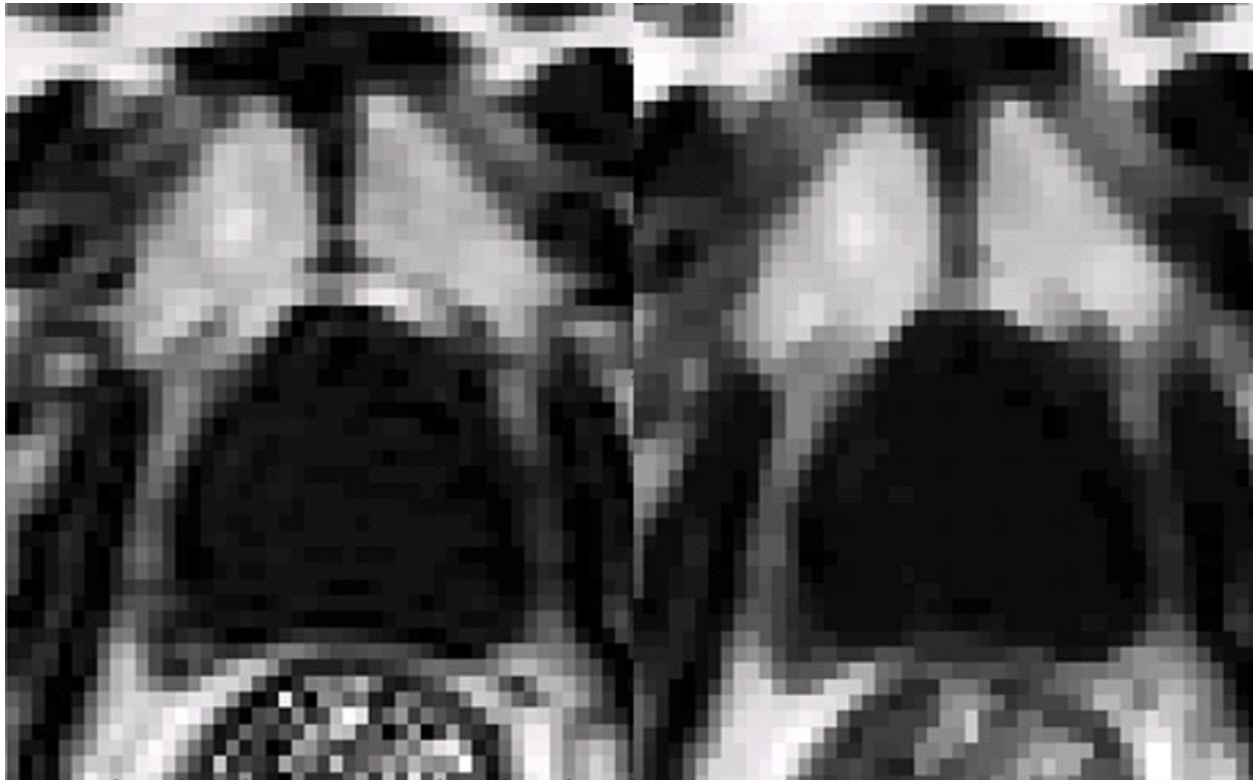


Figure 3: An a) FF_hc map, and b) the same image, median-filtered to smooth the boundaries of the prostate. Dark horizontal lines in the connective tissue of a) become smoothed signal after filtering. **A B**

From the predefined seed point, neighbouring pixels varying less than 5% in intensity from the seed are included in the region. This threshold is standard for region growth[13], and is appropriate to this application given the average range of variation inside the prostate is 0-3.8%--based on values of FF maps from manually segmented ROIs. The goal of the region growth method is to include all portions of the prostate, at

the calculated risk of including areas surrounding the prostate, which can be excluded further in the algorithm.

The region growth outputs both a masked image and an enclosing polygon. A morphological image opening is immediately applied to each slice after region growth, and all regions disconnected from the region containing the seed point are erased. Opening is the process of removing border pixels from an image object—known as erosion—followed by expanding the border of the image object—known as dilation. It has the effect of disconnecting objects joined by a small number of pixels determined by the size of the structuring element. This image opening uses a filled, symmetric 3x3-structuring element. The region growth is then repeated, keeping only the region containing the original seed point, as shown in Figure 4.



Figure 4: A midgland slice in a) original FF map, b) initial region growth output, and c) enclosing polygon after opening. In this slice, the circular rectal wall below to the prostate has invaded the prostate region, and is removed by opening. **A B C**

The enclosing polygon is then interpolated into a 2D spline, curving the edges into a more anatomic shape, as shown in Figure 5. A point-to-point distance array for each point on the polygon is calculated to produce a piecewise cubic spline interpolation. The spline will take the shape that minimizes the order of its governing equations.
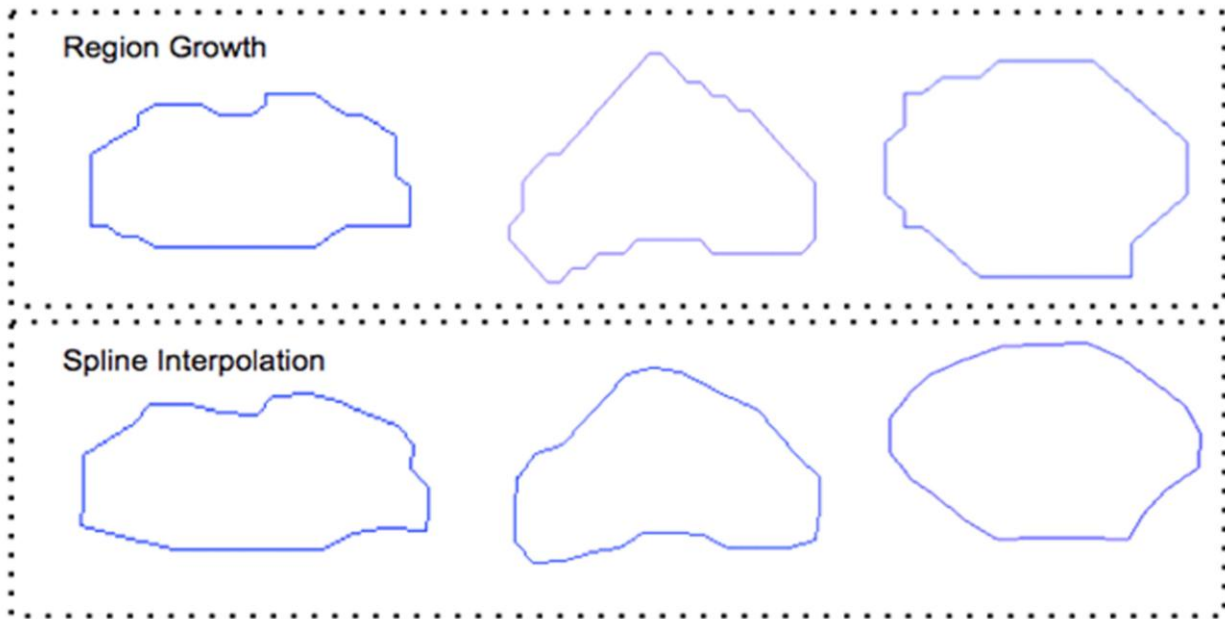
Figure 5: Examples slices of a) apex [from Figure 4], b) midgland, and c) base region growth outputs after opening, and the corresponding d) apex, e) midgland, and f) base splines for those slices.

After each image slice's segmentation undergoes region growth and spline interpolation, the use of 3D information enhances the agreement between slices. As the final semi-automatic step to measure shape agreement between contiguous slices, the spline for each slice is shown and the user selects a reference slice with an accurate segmentation. The slice adjacent to the reference slice—known as the floating slice—is then probed for differences in shape. The basis of determining artifact is the closest Euclidean distance between the each border point on the floating slice and its closest border point on the reference slice. By experimentation, points on the spline with distances to the reference slice border larger than the mean distance by greater than 25% of a standard deviation are typically indicative of image artifact. However, in slices where the distances to the reference border are very similar among floating border points, increases in distance can be indicative of true gland growth, and removing these points can eliminate true prostate border points. By experimentation, only slices with a

12

range of distances greater than 5 pixels typically contain image artifact, as opposed to true growth or shrinkage of the gland between slices. Therefore, only in slices with a range of distances greater than 5 are points possibly erased, as shown in Figure 6. After this comparison, the spline is closed and concatenated with the other slices to prepare for 3D extrusion. The floating slice becomes the reference slice for the next contiguous slice.
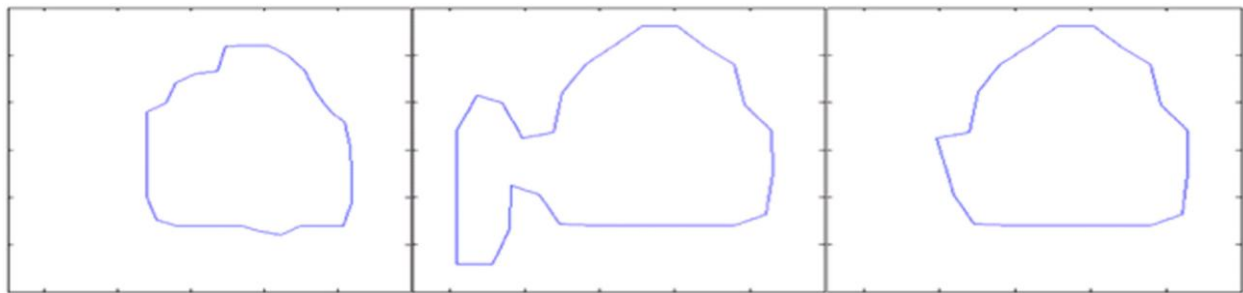


Figure 6: a) The reference slice, b) the floating slice before measuring distances to the reference slice border, and c) the floating slice after removing points of artifact based on distance to the reference slice border. In this example, the range of values was 21.26, and standard deviation was 9.19. Seven points on the floating slice had minimum distance to the reference slice border above 25% of the standard deviation, and were deleted from image (b) to form image (c). **A B C**

Once each slice is probed for artifact, the spline of each slice is converted to a binary image, and the shortest Euclidean distance from the object border is calculated for each pixel, in positive quantities for pixels in the object and negative quantities for pixels in the background. While a binary image only informs whether the pixel belongs to the object or background, this distance transform encodes each pixel with two units of information: belonging to image or background (as positive or negative values), and Euclidean distance from the border between (as the pixel intensity value).

The information added from the distance transform is employed in upsampling the image in three dimensions before display as a completed volume. To upsample, the image pixels are converted to physical space by multiplication with the image resolution.

These 'physical coordinates' are then mapped to a blank image plane of doubled resolution. This method, called forward mapping, is robust in increasing image resolution after acquisition, but can lead to holes in the image if no original pixels map to a given location in the upsampled image. To combat this, the process is accomplished in reverse, with each blank pixel on the upsampled plane converting to physical coordinates and locating the closest pixel in the original image space. This procedure, known as backward mapping, ensures that no pixel in the resulting image plane is blank after registration. Because the algorithm upsamples the image in 3D, an intermediary blank image space is created between each contiguous original image slice. Each pixel is matched to its closest neighbours in its parent image slices, and is linearly interpolated to the intermediary image space, shown in Figure 7. The result increases resolution in the axial image plane as well as along the superior-inferior axis.
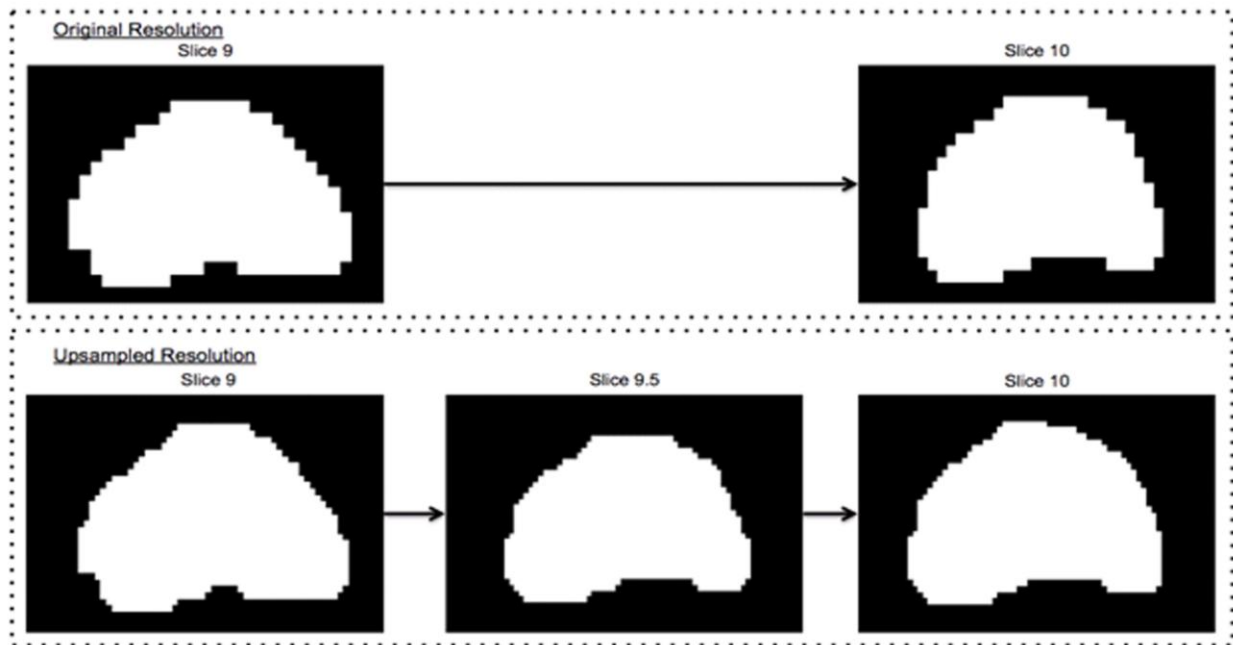


Figure 7: Masked images of the original slice a) 9 and b) adjacent slice 10, input into the upsampling algorithm. Output c) slice 9, d) the new slice (9.5) and e) slice 10 upsampled by a factor of 2. Images c) and e) are generated by upsampling in the axial image plane, and image d) is generated by upsampling in the superior-inferior plane.

Once each slice is upsampled, the slices are displayed as a 3D block—with depth equivalent to slice thickness, and the volume is calculated on the binary image created from the final spline of each slice. The number of pixels equal to 1 in each binary image is totaled and multiplied by the new upsampled image resolution. The volume extrusion, shown in Figure 8, is useful for visualizing the prostate shape, as well as image artifact.
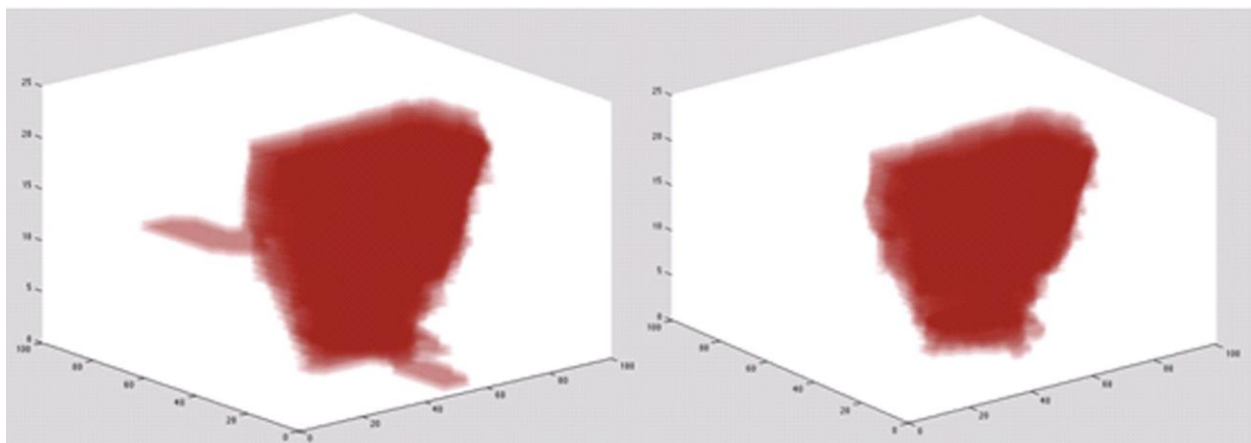


Figure 8: 3D upsampled extrusions shown in isometric projections of a) the prostate segmented by the initial region growth, opening, and spline interpolation, and b) the same prostate after testing the distance of each spline point to a neighboring slice and removing points with distances above the threshold.  A B

Chapter 3: Results and Discussion

There was no significant difference in the volumes recorded from the trial data for the semi-automatic segmentation of the FF_hr map and manual segmentation of the axial T2-weighted image (n=14, p<0.84, paired students t-test). However, the semi-automatic segmentation had a trend to underestimate the size of the prostate gland as compared to the manual segmentation. The mean difference in volume was 5.3 cc with a standard deviation of 7.9 cc. One true outlier had a difference of 39.3 cc (n=14, p<0.01, z=3.19, Grubb's test). By visual inspection, the T2-weighted image of the outlier shows a gland abutting the bladder for several slices. However, the signal difference between the prostate gland and bladder on T2-weighted imaging allows the user to easily determine the prostate boundaries. This is not visible on the FF map because the bladder and prostate both contain very low fat and show similar signal, and is likely responsible for the drastic difference in volumes. Excluding the outlier, the mean difference in volume in the cohort was 3.4 cc, with a standard deviation of 3.3 cc (n=13).

The MR FF_hc map segmentation volumes were significantly different from those of the axial T2-weighted images (n=14, p<0.03, paired student's t-test). By visual inspection, the segmentations of FF_hc maps showed invasion of the psoas muscle into the prostate region during region growth as the most common artifact in this population due to the anatomic proximity and signal similarity. The anatomy of the oblique axial view of the male pelvis on an FF map, as well as artifact removal techniques of opening and comparing distances between borders to erase the psoas muscle, are shown in Figure 9:
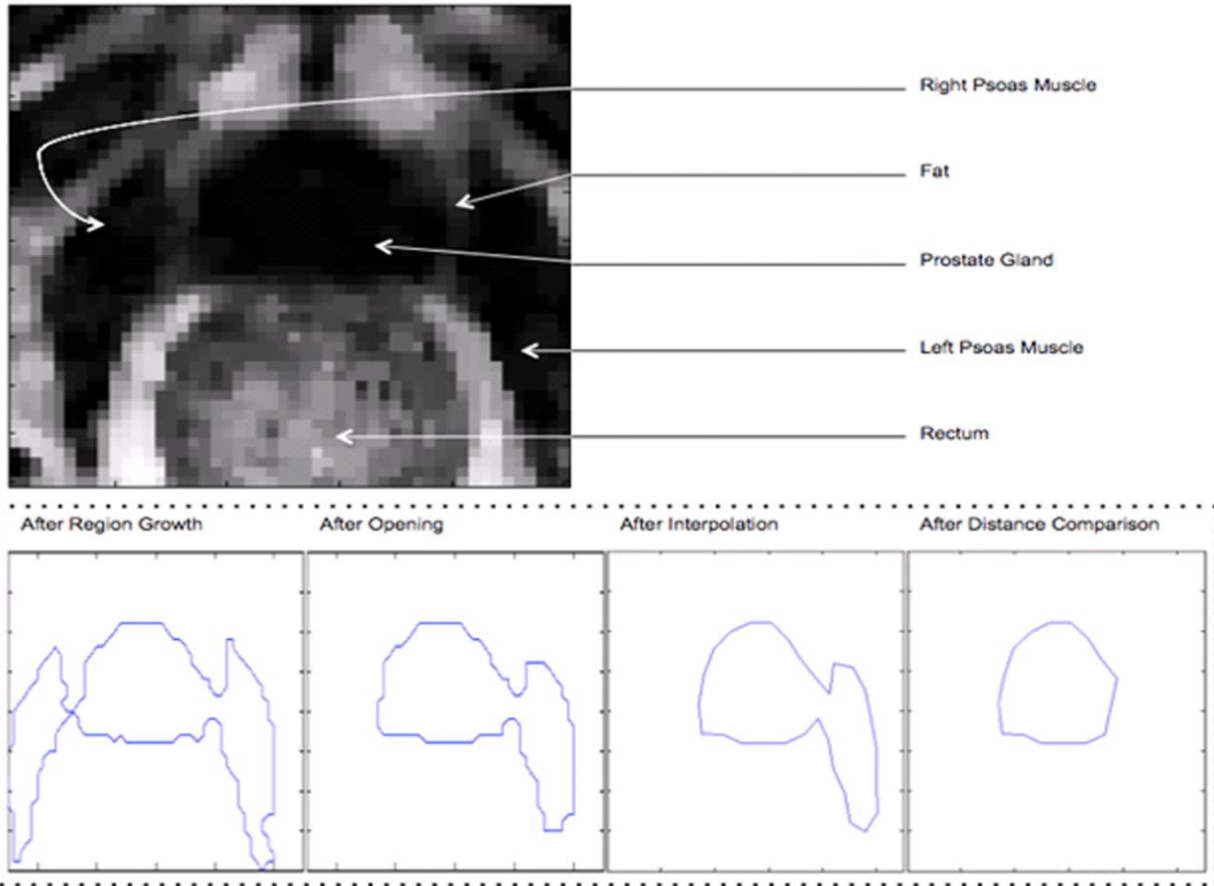
Figure 9: a) An example FF map slice showing the psoas muscles and prostate, along with anatomic markers of the rectum and fat. Output from the algorithm, we see b) both psoas muscles in the prostate region after region growth, c) the right psoas removed by image opening, d) the border smoothed by spline interpolation, and e) the left psoas removed after comparing distances with a reference slice.

While some of these were removed in the image opening and distance comparison, some non-prostatic regions were included in the final volume, as shown in Figure 10. The increased resolution of the FF_hr map better differentiates the fat surrounding the prostate, leading to more accurate segmentations, and a more well-defined border between the prostate and psoas. This is primarily due to partial voluming effect: signals from two structures in a single voxel will merge into an averaging of the two structures' signal intensities. Although the bigger voxels in the FF_hc map show a higher signal-to-noise ratio (SNR) in voxels within organs, the voxels that straddle the

17

prostate border and fatty tissue have a mix of signals and show weaker signal enhancement from the fat. On the FF_hr map, because the voxels are smaller, there is a larger chance of having voxels composed entirely of fat, forming a distinct border.
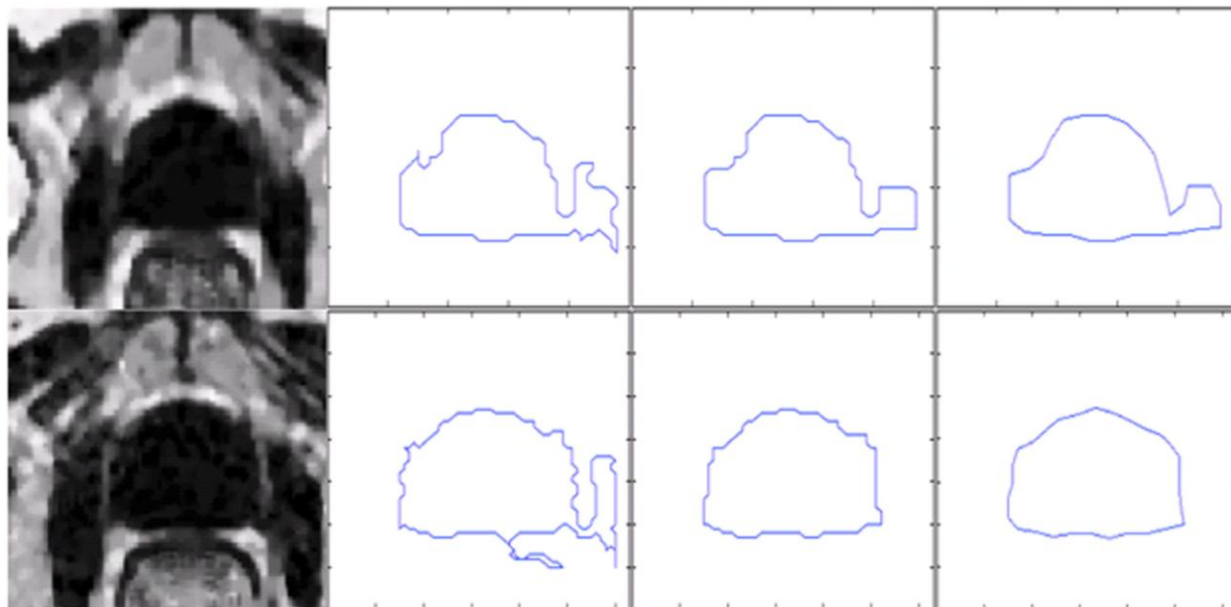


Figure 10: In an example slice, a) the FF_hc map, b) the initial region growth, c) the region after opening, and d) the region after interpolation and border distance testing with a portion of the left psoas muscle in the prostate region. The e) FF_hr map, f) initial region growth showing left psoas invasion as well as rectal invasion, g) the region after opening, with the psoas and rectum removed from the image, and h) the interpolated shape. The fat between the prostate and psoas muscle is easily visible in the FF_hr map (e) and less defined in the FF_hc map (a).

While the FF_hc maps increase prostate definition in 2D slices, they do not correct the signal similarity between the prostate and bladder. Because neither gland contains fat, both appear with very low signal intensities on any FF map. In cases where the prostate abuts the bladder, the prostate size can be grossly overestimated. Determination of a correction factor between either FF map segmentation and manual T2-weighted image segmentation is not feasible based on this dataset due to the range of segmentation differences.

As visible in Figure 11, the FF_hc maps led to a consistently overestimated prostate volume. This is likely because the undifferentiated psoas muscle increased individual slice areas. However, the FF_hr maps have a close correlation with the manual segmented. In the outlier case, number 13, these maps overestimate the prostate volume when the prostate base extends into the bladder.
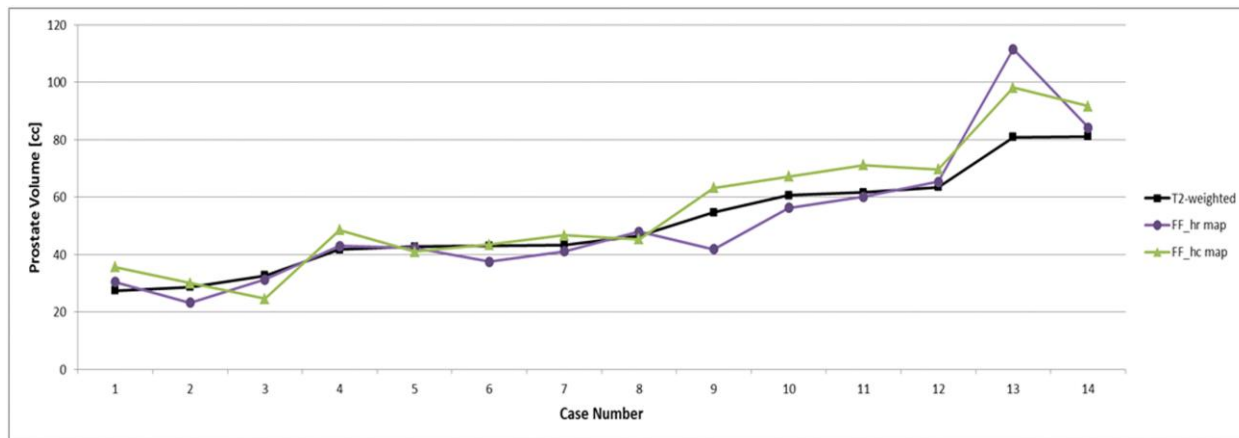


Figure 11: The final volumes of high-contrast (hc) and high-resolution (hr) FF map images compared with the manually-segmented volumes on T2-weighted images.

The manual segmentation on the corresponding T2-weighted image is sensitive to the edge of the prostate adjacent to the bladder in the base as well as where the urethra extends past the apex. Motion artifact was not present in T2-weighted images of any of the patients in this population, leading to a reliable standard against which the semi-automatic segmentation can be measured. However, the T2-weighted image and he IDEAL scans were separated by approximately 23 minutes during each scan, and both movement of the patient and filling of the bladder between these scans may account for perceived differences in prostate size.

Prior segmentation methods in the literature have used atlas-based models to define the prostatic boundaries[14,15,16,17]. However, most methods consistently underestimate the prostatic volume[15,16,17]. A popular technique is to estimate the

prostate size based on a midgland slice, which does not translate well to abnormally shaped prostates[15,16] or in the presence of image artifact. The slice chosen is also a major factor in the size estimation. It is also typical for segmentation methods to include the seminal vesicles, as they are located adjacent to the prostate and are of similar intensity on most images[14,17]. However the size of the seminal vesicles has no clinical importance, and no functional information is gained by adding seminal vesicles to the size[14]. Segmentation methods from the literature also commonly use volunteer data in testing[15,16], which differs from patient data both in average size and symmetry. Abnormal prostate growth, from prostate cancer or BPH, can cause the prostate to take an asymmetric shape, making atlases based on volunteer data prone to false segmentation in a diseased population. Although varying in approach, all of these techniques become less accurate in large or abnormally shaped prostates[14,15,16,17].

Recently, an industry-created approach to semi-automatic prostate segmentation has become available to clinical sites[18]. This segmentation consists of an algorithmic estimation of prostate size followed by an option for clinical practitioners to modify the shape. This approach is easily usable, however the software fundamentally limits the modification allowable by a user. Manual alterations must be at least 5 mm in distance, and cannot exceed a curvature of 50° [18]. Additionally, the software cannot be implemented in real-time, meaning a segmentation useful for aligning prescriptions during the MR examination or a biopsy procedure is not feasible. Furthermore, it is not possible to extract the shape boundaries to use the shape outside of the software. Therefore experimental research methods, such as combining with a time lapse of

perfusion enhancement or a longitudinal study of growth in a single patient cannot be explored.

Most segmentation algorithms utilize a T2-weighted image[14,15,16,17,18]. For the proposed technique, the fat fraction map was selected due to the bright signal from fat bordering the prostate, and low signal intensity inside the prostate. While robust methods exist for estimating prostate volume, this method may be implementable in real-time applications, has a prostate mold that is extractable from the algorithm for research purposes, and is available as an open source platform.

Chapter 5: Future Work

To use the current FF map for a reliable segmentation of the prostate, the most important improvement is an estimation of the volume if the base of the prostate abuts the bladder. Inclusion of the bladder or exclusion of the base of the prostate leads to grossly over or underestimated prostate volumes, respectively. However, abdominal organs move significantly during MR scans, and registering on a steady object like the femoral head or rectum does not necessarily register the prostate gland. Furthermore, the bladder is likely to fill between the acquisition of the T2-weighted image and the IDEAL sequence which generates the FF map. Alignment could be improved by acquiring these two scans in succession. Alternatively, the curvature of the base can be estimated by the sizes of consecutive midgland slices. However, because the prostate shape is very deformable, this modeling is unlikely to account for growth abnormalities in the base. During the semi-automatic segmentation, users could select the region to include the prostate and bladder to avoid underestimation of the volume. Existing software to register T2-weighted images and functional techniques based on rectal alignments will be used to register the FF map to the T2-weighted image. Multiplying the binary mask of the segmentation to a registered T2-weighted image will allow a second region growth to separate the bladder and prostate gland by intensity.

It is also necessary to test the proposed segmentation algorithm on a large number of patients with various treatments for prostate cancer. In particular, transurethral resection of the prostate (TURP) poses an issue for current segmentation algorithms[14,15,16,17,18]. This is typically due to the inability to distinguish where the prostate apex begins, and the wide range of intensities and shapes of the urethra after

the surgery. On the FF map, the urethra has a very similar intensity to the prostate, leading to an easier registration for the proposed algorithm. However, this acquisition has not been tested on a patient after TURP.

Brachytherapy seed implants also cause distortion and wide ranges of intensities within the prostate gland, and can cause segmentation failures in current algorithms[14,15,16,17,18]. However, this acquisition has not been tested on a patient with brachytherapy seed implants.

Inclusion of the bladder or surrounding structures in treated or large and abnormal glands does not hinder the algorithm from being used in localization during MR-guided prostate biopsies. This procedure currently uses qualitative methods of localization by trained personnel, and could likely benefit greatly from the inclusion of localization and boundaries of the prostate and bladder for use during prescription.

<u>Conclusion</u>

The proposed segmentation algorithm using the FF_hr map creates a reliably accurate prostate volume in this population. As part of an mpMRI exam, the segmentation is particularly useful for localization of the prostate gland relative to functional data. This technique should be tested in an extensive population including patients on a variety of treatment regimens, and should be explored further.

References:

1. Cancer Facts and Figures 2013. Atlanta, GA: American Cancer Society; 2013. Available from http://www.cancer.org/research/cancerfactsfigures/cancerfactsfigures/cancer-facts-figures-2013

2. Ito, Kazuto, Mai Miyakubo, Yoshitaka Sekine, Hidekazu Koike, Hiroshi Matsui, Yasuhiro Shibata, and Kazuhiro Suzuki. "Diagnostic Significance of [−2]pro-PSA and Prostate Dimension-adjusted PSA-related Indices in Men with Total PSA in the 2.0–10.0 ng/mL Range." *World Journal of Urology* 31.2 (2013): 305-11.

3. Kurhanewicz J, Vigneron D, Carroll P, Coakley F. Multiparametric magnetic resonance imaging in prostate cancer: present and future. Curr Opin Urol 2008;18(1):71-77.Weiss, Brian E., Alan J. Wein, S. Bruce Malkowicz, and Thomas J. Guzzo. "Comparison of Prostate Volume Measured by Transrectal Ultrasound and Magnetic Resonance Imaging: Is Transrectal Ultrasound Suitable to Determine Which Patients Should Undergo Active Surveillance?" *Urologic Oncology: Seminars and Original Investigations* 31.8 (2013): 1436-440.

4. Cooperberg, Matthew R., Jeanette M. Broering, Mark S. Litwin, Deborah P. Lubeck, Shilpa S. Mehta, James M. Henning, and Peter R. Carroll. "The Contemporary Management Of Prostate Cancer In The United States: Lessons From The Cancer Of The Prostate Strategic Urologic Research Endeavor (Capsure), A National Disease Registry." *The Journal of Urology* 171.4 (2004): 1393-401.

5. Lewin, J. S., J. L. Duerk, V. R. Jain, C. A. Petersilge, C. P. Chao, and J. R. Haaga. "Needle Localization in MR-guided Biopsy and Aspiration: Effects of Field Strength, Sequence Design, and Magnetic Field Orientation." *American Journal of Roentgenology* 166.6 (1996): 1337-345.

6. Common physician sizing

7. Noworolski SM, Crane JC, Vigneron DB, Kurhanewicz J. A clinical comparison of rigid and inflatable endorectal-coil probes for MRI and 3D MR spectroscopic imaging (MRSI) of the prostate. J Magn Reson Imaging 2008;27(5):1077-1082

8. Stevens, K. J., R. F. Busse, E. Han, A. C. S. Brau, P. J. Beatty, C. F. Beaulieu, and G. E. Gold. "Ankle: Isotropic MR Imaging with 3D-FSE-Cube--Initial Experience in Healthy Volunteers." *Radiology* 249.3 (2008): 1026-033.

9. Hambrock, T., D. M. Somford, H. J. Huisman, I. M. Van Oort, J. A. Witjes, C. A. Hulsbergen-Van De Kaa, T. Scheenen, and J. O. Barentsz. "Relationship between Apparent Diffusion Coefficients at 3.0-T MR Imaging and Gleason Grade in Peripheral Zone Prostate Cancer." *Radiology* 259.2 (2011): 453-61.

10. Puech, Philippe, Eric Potiron, Laurent Lemaitre, Xavier Leroy, Georges-Pascal Haber, Sebastien Crouzet, Kazumi Kamoi, and Arnauld Villers. "Dynamic Contrast-enhanced–magnetic Resonance Imaging Evaluation of Intraprostatic Prostate Cancer: Correlation with Radical Prostatectomy Specimens." *Urology* 74.5 (2009): 1094-099. Web.

11. Umbehr, Martin, Lucas M. Bachmann, Ulrike Held, Thomas M. Kessler, Tullio Sulser, Dominik Weishaupt, John Kurhanewicz, and Johann Steurer. "Combined Magnetic Resonance Imaging and Magnetic Resonance Spectroscopy Imaging in the Diagnosis of Prostate Cancer: A Systematic Review and Meta-analysis." *European Urology* 55.3 (2009): 575-91. Web.

12. Reeder, Scott B. Iterative Decomposition with Echo Asymmetry and Least-Squares Estimation. General Electric, assignee. Patent 6,856,134. 23 May 2003.

13. Kellner, Daniel. *RegionGrowing.m*. Computer software. *Region Growing (2D/3D) Grayscale*. Vers. 1. BSD, 2011. Web.

14. Dowling, J. A. "Fast Automatic Multi-atlas Segmentation of the Prostate from 3D MR Images." *Prostate Cancer Imaging* 6963 (2011): 10-21.

15. Klein, S. "Segmentation of the Prostate in MR Images by Atlas Matching." *2007 4th IEEE International Symposium on Biomedical Imaging: From Nano to Macro*(2007): 1300-303. Print.

16. Zwiggelaar, R., Y. Zhu, and S. Williams. "Semi-automatic Segmentation of the Prostate. "*Pattern Recognition and Image Analysis* 2652 (2003): 1108-116.

17. Klein, Stefan, Uulke A. Van Der Heide, Irene M. Lips, Marco Van Vulpen, Marius Staring, and Josien P. W. Pluim. "Automatic Segmentation of the Prostate in 3D MR Images by Atlas Matching Using Localized Mutual Information." *Medical Physics* 35.4 (2008): 1407.

18. *Dynacad for Prostate*. Computer software. 580243 *Invivo Corporation*. Rev 3. N.p., 2013.

Appendix I: Definitions

BPH: Benign Prostatic Hyperplasia
DCE: Dynamic Contrast-Enhanced Imaging
DWI: Diffusion-Weighted Imaging
FF: Fat Fraction
FF_hc: The FF map made from the IDEAL sequence for high contrast
FF_hr: The FF map made from the IDEAL sequence for high resolution
FSE: Fast Spin-Echo
IDEAL: Iterative Decomposition and Echo Asymmetry with Least-squares Estimation
IDEAL_hc: The IDEAL sequence with parameters optimized for high contrast
IDEAL_hr: The IDEAL sequence with parameters optimized for high resolution
mpMRI: Multiparametric MRI
MR: Magnetic Resonance
MRI: Magnetic Resonance Imaging
PSA: Prostate-Specific Antigen
ROI: Region Of Ineterest
SNR: Signal-to-Noise Ratio
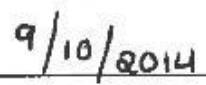TURP: TransUrethral Resection of the Prostate

## Publishing Agreement

*It is the policy of the University to encourage the distribution of all theses, dissertations, and manuscripts. Copies of all UCSF theses, dissertations, and manuscripts will be routed to the library via the Graduate Division. The library will make all theses, dissertations, and manuscripts accessible to the public and will preserve these to the best of their abilities, in perpetuity.*

## Please sign the following statement:

*I hereby grant permission to the Graduate Division of the University of California, San Francisco to release copies of my thesis, dissertation, or manuscript to the Campus Library to provide access and preservation, in whole or in part, in perpetuity.*

_Natalie Rom_

Author Signature

9/10/2014

Date